Journal of Solid State Chemistry 182 (2009) 3131–3137

Contents lists available at ScienceDirect

Journal of Solid State Chemistry

journal homepage: www.elsevier.com/locate/jssc

$Ba_5Ti_{12}Sb_{19+x}$, a polar intermetallic compound with a stuffed γ-brass structure

Haiying Bie, Arthur Mar *

Department of Chemistry, University of Alberta, Edmonton, Alberta, Canada T6G 2G2

ARTICLE INFO

Article history:
Received 30 June 2009
Received in revised form
26 August 2009
Accepted 30 August 2009
Available online 9 September 2009

Keywords:
Intermetallics
Crystal structure
Antimonide

ABSTRACT

The polar intermetallic compound $Ba_5Ti_{12}Sb_{19+x}$ ($x \leqslant 0.2$) has been synthesized by reaction of the elements. Single-crystal X-ray diffraction analysis revealed that it adopts a new structure type ($Ba_5Ti_{12}Sb_{19.102(6)}$, space group $P4\bar{3}m$, $Z=2$, $a=12.4223(11)$ Å, $V=1916.9(3)$ Å^3). The set of Ba and Sb sites corresponds to the structure of Cu_9Al_4, a γ-brass type with a primitive cell. A complex three-dimensional framework of Ti atoms, in the form of linked planar Ti_9 clusters, is stuffed within the γ-brass-type Ba–Sb substructure. Notwithstanding its relationship to the γ-brass structure, the compound does not appear to conform to the Hume–Rothery electron concentration rules. Band structure calculations on an idealized $Ba_5Ti_{12}Sb_{19}$ model suggest that the availability of bonding states above the Fermi level is responsible for the partial occupation, but only to a limited degree, of an additional Sb site within the structure. Magnetic measurements indicated Pauli paramagnetic behaviour.

1. Introduction

Although an important driving force for the study of solid-state antimonides stems from their many potentially useful materials applications, a more fundamental reason is simply the fascination for their bonding character, related to the intermediate position of Sb within the p-block elements [1–4]. In combination with more electropositive metals, these antimonides can be considered to be polar intermetallic phases, many of whose structures can be understood as though full electron transfer were taking place (Zintl–Klemm concept) [5]. As part of an ongoing effort to understand the solid-state chemistry of Sb, we have been investigating the synthesis and structures of new ternary rare-earth antimonides. In particular, within the *RE*–Ti–Sb systems, the existence of three series of phases has been revealed: RE_3TiSb_5 (*RE*=La–Nd, Sm) [6,7], $RE_2Ti_7Sb_{12}$ (*RE*=La–Nd) [8], and $RE_2Ti_{11-x}Sb_{14+x}$ (*RE*=Sm, Gd, Tb, Yb) [9]. The limited range of *RE* substitution permitted for these different series implies that the size of the *RE* atom may be one factor that controls their formation. Interestingly, the $RE_2Ti_{11-x}Sb_{14+x}$ series does not form for the intervening *RE* elements (Dy, Ho, Er, Tm) between Tb and Yb. In fact, the unit cell for $Yb_2Ti_{11-x}Sb_{14+x}$ is actually larger than those for the earlier *RE* elements (Sm, Gd, Tb), suggesting the presence of mixed-valent Yb^{2+} and Yb^{3+}. If so, could Yb be substituted by other electropositive divalent elements?

We have attempted the synthesis of ternary alkaline-earth-containing antimonides in the *AE*–Ti–Sb (*AE*=Ca, Sr, Ba) systems and report herein the discovery of the compound $Ba_5Ti_{12}Sb_{19+x}$. The structure type is new and unusual, because it combines features that are reminiscent of intermetallic phases of little or no polarity (Hume–Rothery phases) [10] with the simultaneous occurrence of homoatomic Ti–Ti and Sb–Sb bonding, which at first glance seems to be rationalizable on the basis of the Zintl–Klemm concept [11]. Band structure calculations have been performed to provide further understanding for the stability of this compound.

2. Experimental

2.1. Synthesis

On the basis of the existence of the rare-earth antimonides $RE_2Ti_7Sb_{12}$ and $RE_2Ti_{11-x}Sb_{14+x}$, initial attempts to prepare analogous phases containing alkaline-earth metals in the *AE*–Ti–Sb (*AE*=Ca, Sr, Ba) systems were confined to similar compositions. Along with byproducts of binary phases ($BaSb_2$ and $TiSb_2$), a new ternary phase was identified in a reaction with loading stoichiometry "$Ba_9Ti_{34}Sb_{57}$", prepared by combining the elements (Ba pieces, 99.9%, British Drug House; Ti powder, 99.98%, Cerac; Sb powder, 99.995%, Cerac) placed in alumina crucibles within evacuated fused-silica tubes. The heating profile was the same as that used in the preparation of $RE_2Ti_7Sb_{12}$ or $RE_2Ti_{11-x}Sb_{14+x}$ [8,9]:

* Corresponding author. Fax: +1 780 492 8231.
E-mail address: arthur.mar@ualberta.ca (A. Mar).

0022-4596/$ - see front matter © 2009 Elsevier Inc. All rights reserved.
doi:10.1016/j.jssc.2009.08.030

the tubes were heated from room temperature to 650 °C over 1 day, heated to 1050 °C for 1 day, kept at that temperature for 2 days, slowly cooled to 800 °C over 4 days, kept at that temperature for 12 days, and then slowly cooled to 20 °C over 4 days. (The high volatility of Ba renders arc-melting an unsuitable preparative method.) These reactions yielded black block-shaped single crystals, whose surface tends to degrade upon exposure to air in the course of 1 h. Determining their chemical composition by energy-dispersive X-ray (EDX) analysis, performed on a Hitachi S-2700 scanning electron microscope, was impracticable because of the overlap of Ba and Ti peaks. X-ray photoelectron spectroscopy, performed on a Kratos Axis Ultra spectrometer equipped with a monochromatic Al Kα X-ray source, did confirm the presence of all three elements Ba, Ti, and Sb, but a quantitative analysis was not possible because of the partial reduction of Ti that occurred in the course of the Ar^+ sputtering process. Further syntheses, performed after the crystal structure was determined (see later), established the composition to be $Ba_5Ti_{12}Sb_{19+x}$, where x is a small number. Similar reactions were carried out for *AE*=Ca and Sr. For *AE*=Ca, the reaction yielded the binary phases $TiSb_2$, Ti_5Sb_8, and $CaSb_2$; for *AE*=Sr, a different ternary phase was identified whose structure refinement is in progress.

2.2. Structure determination

Single-crystal X-ray diffraction data were collected on a Bruker Platform/SMART 1000 CCD diffractometer at 22 °C using ω scans. Structure solution and refinement were carried out with use of the SHELXTL (version 6.12) program package [12]. Face-indexed numerical absorption corrections were applied. Crystal data and further details of the data collection are given in Table 1.

Inspection of the intensity data suggested the cubic space groups $Pm\bar{3}$, $Pm\bar{3}m$, and $P4\bar{3}m$. Application of direct methods revealed that a reasonable solution could be obtained in space group $P4\bar{3}m$. After the positions of all atoms in the structural model "$Ba_5Ti_{12}Sb_{19}$" were identified and refined, the difference electron density map revealed a residual peak of 7.1e$^-$/Å^3. The initial thought was that this peak could be assigned as an O atom, perhaps originating adventitiously from the fused-silica tube. However, the distances from this peak to the nearest-neighbour Sb (2.81 Å) or Ba atoms (3.37 Å) are far too long compared to typical Sb–O (1.8–2.3 Å in binary antimony oxides) or Ba–O contacts (2.5–2.9 Å in binary barium oxides), respectively [13]. On the other hand, because the distances are appropriate for Sb–Sb or Ba–Sb contacts, this site was assigned to be partially occupied by Sb atoms. The occupancy of this Sb6 site, when refined, converged to 0.051(3).

The occurrence of this partially occupied Sb6 site was supported by additional evidence. First, the same difference electron density peak persisted when other space groups, such as $Pm\bar{3}$, were tested. Second, X-ray diffraction data were collected for other crystals obtained under different reaction conditions: (i) the original preparation, "$Ba_9Ti_{34}Sb_{57}$", which is Sb-rich with respect to that of the structural model, (ii) the loading composition similar to the structural model, "$Ba_5Ti_{12}Sb_{19}$", and (iii) the loading composition "$Ba_5Ti_{12}Sb_{19}$" in the presence of Sn flux. The refinement results for these three crystals were essentially identical (Table 1), with the same partially occupied Sb6 site present. Except for the crystal grown in the presence of Sn flux, the Flack parameters were close to zero, indicating the occurrence of one absolute configuration. Third, additional syntheses were performed with different amounts of excess Sb in "$Ba_5Ti_{12}Sb_{19+x}$" (x=0, 0.2, 1.0, 2.0). The products were analyzed by their powder X-ray diffraction (XRD) patterns measured on an Inel powder diffractometer equipped with a CPS 120 detector (Fig. S1 in Supporting Information). The products were quantitatively pure in the reactions with x=0 and 0.2, with XRD patterns that were in excellent agreement with those simulated from the single-crystal structural model, whereas other binary phases ($BaSb_2$ and $TiSb_2$) appeared in the reactions with x=1.0 and 2.0. This result implies that the Sb6 site cannot sustain a full occupancy; the maximum occupancy is estimated to be 10%, consistent with the refined compositions of the crystals examined above.

Atomic positions were standardized with the program STRUCTURE TIDY [14]. Final values of the positional and displacement parameters, for the crystal grown in the absence of Sn flux, are given in Table 2. Selected interatomic distances are listed in

Table 1
Crystallographic data for $Ba_5Ti_{12}Sb_{19+x}$.

Crystal[a]	**1**	**2**	**3**
Formula	$Ba_5Ti_{12}Sb_{19.176(6)}$	$Ba_5Ti_{12}Sb_{19.098(6)}$	$Ba_5Ti_{12}Sb_{19.102(6)}$
Formula mass (amu)	3596.06	3586.93	3586.93
Space group	$P\bar{4}3m$ (No. 215)	$P\bar{4}3m$ (No. 215)	$P\bar{4}3m$ (No. 215)
a (Å)	12.4242(7)	12.4236(7)	12.4223(11)
V (Å^3)	1917.8(2)	1917.5(2)	1916.9(3)
Z	2	2	2
ρ_{calcd} (g cm^{-3})	6.227	6.212	6.214
Crystal dimensions (mm)	0.13 × 0.12 × 0.04	0.13 × 0.11 × 0.09	0.20 × 0.17 × 0.04
μ(Mo $K\alpha$) (mm^{-1})	20.60	20.55	20.56
Transmission factors	0.0966–0.4816	0.1013–0.2188	0.0642–0.4209
2θ range (deg.)	4.64–66.14	4.64–66.26	4.64–66.26
No. of data collected	26490	26616	26701
No. of unique data, including $F_o^2<0$	1423 (R_{int}=0.077)	1435 (R_{int}=0.057)	1430 (R_{int}=0.051)
No. of unique data, with $F_o^2 > 2\sigma(F_o^2)$	1377	1407	1414
No. of variables	46	47	47
Flack parameter	0.00(5)	0.36(5)	0.04(5)
$R(F)$ for $F_o^2 > 2\sigma(F_o^2)$[b]	0.024	0.022	0.018
$R_w(F_o^2)$[c]	0.048	0.048	0.045
Goodness of fit	1.124	1.101	1.174
$(\Delta\rho)_{max}$, $(\Delta\rho)_{min}$ (e Å^{-3})	2.16, −2.51	3.53, −1.86	3.56, −1.82

[a] Synthetic conditions: (**1**) "$Ba_9Ti_{34}Sb_{57}$", (**2**) "$Ba_5Ti_{12}Sb_{19}$" in presence of Sn flux, and (**3**) "$Ba_5Ti_{12}Sb_{19}$" in absence of Sn flux.
[b] $R(F)=\sum||F_o|-|F_c||/\sum|F_o|$.
[c] $R_w(F_o^2)=[\sum[w(F_o^2-F_c^2)^2]/\sum wF_o^4]^{1/2}$; $w^{-1}=[\sigma^2(F_o^2)+(Ap)^2+Bp]$ where $p=[\max(F_o^2,0)+2F_c^2]/3$.

Table 3. Further data, in CIF format, have been sent to Fachinformationszentrum Karlsruhe, Abt. PROKA, 76344 Eggenstein-Leopoldshafen, Germany, as supplementary material No. CSD-380356 and can be obtained by contacting FIZ (quoting the article details and the corresponding CSD numbers).

Table 2
Atomic coordinates and equivalent isotropic displacement parameters for $Ba_5Ti_{12}Sb_{19.102(6)}$.

Atom	Wyckoff position	x	y	z	U_{eq} (Å^2)[a]
Ba1	6*g*	0.17193 (5)	½	½	0.0206 (1)
Ba2	4*e*	0.83534 (3)	x	x	0.0179 (1)
Ti1	12*i*	0.16027 (5)	x	0.32768(7)	0.0095 (2)
Ti2	12*h*	0.18670 (7)	½	0	0.0096 (2)
Sb1	12*i*	0.21922 (2)	x	0.54253(3)	0.01281 (7)
Sb2	12*i*	0.33151 (2)	x	0.01001(3)	0.01065 (7)
Sb3	6*f*	0.36252 (4)	0	0	0.00915 (8)
Sb4	4*e*	0.11252 (3)	x	x	0.0124 (1)
Sb5	4*e*	0.32147 (3)	x	x	0.0114 (1)
Sb6[b]	4*e*	0.6354 (5)	x	x	0.009 (3)

[a] U_{eq} is defined as one-third of the trace of the orthogonalized U_{ij} tensor.
[b] Occupancy of 0.051(3).

Table 3
Selected interatomic distances in $Ba_5Ti_{12}Sb_{19.102(6)}$.

Ba1–Sb6 (× 2)	3.374 (2)	Ti1–Sb4	2.8013 (11)
Ba1–Sb1 (× 4)	3.5763 (4)	Ti1–Sb2 (× 2)	2.8304 (4)
Ba1–Sb2 (× 2)	3.5788 (6)	Ti1–Sb5	2.8330 (10)
Ba1–Sb5 (× 2)	3.6452 (5)	Ti1–Sb3	2.8486 (9)
Ba1–Sb2 (× 2)	3.7243 (6)	Ti1–Sb1	2.8628 (10)
Ba2–Sb4 (× 3)	3.5629 (6)	Ti2–Sb2 (× 2)	2.7627 (6)
Ba2–Sb2 (× 3)	3.6469 (5)	Ti2–Sb1 (× 2)	2.8032 (4)
Ba2–Sb1 (× 3)	3.7616 (7)	Ti2–Sb3 (× 2)	2.8801 (8)
Ba2–Sb3 (× 3)	3.7959 (5)	Ti1–Ti1 (× 2)	2.9410 (15)
Sb6–Sb1 (× 3)	2.803 (6)	Ti1–Ti2 (× 2)	2.9417 (8)
Sb5–Sb1 (× 3)	3.2814 (4)	Ti2–Ti2 (× 2)	3.2798 (12)

2.3. Band structure calculation

Tight-binding linear muffin tin orbital (TB-LMTO) band structure calculations were performed on the idealized $Ba_5Ti_{12}Sb_{19}$ structure, in which the Sb6 site is neglected, within the local density and atomic spheres approximations using the Stuttgart TB-LMTO program [15]. The basis sets consisted of Ba 6*s*/6*p*/5*d*/4*f*, Ti 4*s*/4*p*/3*d*, and Sb 5*s*/5*p*/5*d*/4*f* orbitals, with the Ba 6*p*, Ti 4*p*, and Sb 5*d*/4*f* orbitals being downfolded. Integrations in reciprocal space were carried out with an improved tetrahedron method over 24 independent k points within the first Brillouin zone. For comparison, a calculation on a hypothetical $Ba_5Ti_{12}Sb_{21}$ model with fully occupied Sb6 sites was also performed in a similar fashion.

2.4. Magnetic properties

Measurements of dc magnetic susceptibility were made on a 3.64 mg ground sample of $Ba_5Ti_{12}Sb_{19+x}$ between 2 and 300 K on a Quantum Design 9T-PPMS dc magnetometer/ac susceptometer under an applied field of 0.5 T. Susceptibility values were corrected for contributions from the holder and sample diamagnetism.

3. Results and discussion

Although many ternary alkaline-earth antimonides *AE*–*M*–Sb have now been reported, these are largely restricted to compounds where *M* is a mid-to-late transition metal or a post-transition metal (e.g., $Ba_3Cd_2Sb_4$ [16], $AE_{21}Mn_4Sb_{18}$ [17,18], $AE_{14}MSb_{11}$ [19], $SrSn_3Sb_4$ [20]). The new compound $Ba_5Ti_{12}Sb_{19+x}$

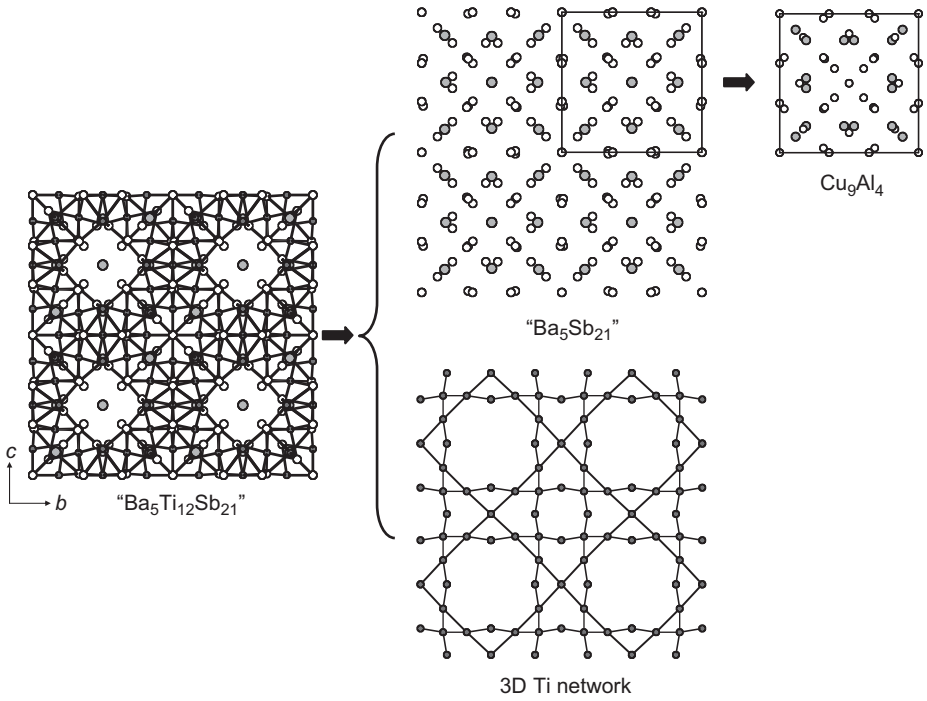

Fig. 1. Projection of idealized "$Ba_5Ti_{12}Sb_{21}$" (with Sb6 site taken to be completely occupied) in a polyhedral representation highlighting $TiSb_6$ octahedra (left). The large lightly shaded circles are Ba atoms, the small solid circles are Ti atoms, and the medium open circles are Sb atoms. The structure can be decomposed into a "Ba_5Sb_{21}" substructure and a 3D network of Ti atoms (centre). The "Ba_5Sb_{21}" substructure is isopointal to Cu_9Al_4, a γ-brass structure (top right).

is the first example, to our knowledge, where M is an early transition metal in these systems. The non-stoichiometry arises from partial occupation of the Sb6 site (up to ~10%), corresponding to a phase width with a maximum of x=0.2, and is understandable from structural and electronic reasons, discussed later.

A conventional description in terms of M-centred polyhedra is not particularly illuminating. Two types of $TiSb_6$ octahedra, with Ti–Sb distances (2.763–2.880 Å) similar to those found in other Ti-containing antimonides (e.g., Ti_2Sb, 2.786–2.856 Å [21]; $La_2Ti_7Sb_{12}$, 2.737–2.879 Å [8]), are connected through face-sharing to form a complicated 3D arrangement defining cavities that are filled by the Ba atoms (Fig. 1). A more elegant approach starts by considering the idealized composition "$Ba_5Ti_{12}Sb_{21}$" in which the Sb6 site is taken to be fully occupied. The structure can then be decomposed into two parts (Fig. 1). The "Ba_5Sb_{21}" (Z=2) substructure is isopointal to Cu_9Al_4 (Z=4), a γ-brass structure with a primitive unit cell [22–24]. The Ti atoms form a 3D network that permeates through the "Ba_5Sb_{21}" substructure. From this standpoint, the cubic γ-brass "Ba_5Sb_{21}" substructure is easily visualized in terms of two types of clusters, one positioned at the origin and another at the body centre, in a CsCl-type arrangement (Fig. 2a), hence the primitive cell. (In the I-centred cell of γ-brass itself, Cu_5Zn_8, the two clusters are identical [25].) Using the well-developed terminology for γ-brass structures [26–28], we can identify each of the 26-atom clusters as being composed of an inner tetrahedron (IT) surrounded by an outer tetrahedron (OT) surrounded by an octahedron (OH) surrounded by a cuboctahedron (CO) (Fig. 3). The two clusters differ in the location of the Ba atoms (OT vs. OH). This densely packed atomic arrangement of Ba and Sb atoms leads to reasonable Ba–Sb (3.563–3.796 Å) and Sb–Sb separations (3.28 Å and longer), except for the case of the partially occupied Sb6 site. Sandwiched between staggered triangles of three Ba1 and three Sb1 atoms, the Sb6 site resides within a highly flattened octahedron, giving distances (Sb6–Ba1, 3.374 Å; Sb6–Sb1, 2.803 Å) that are scarcely longer than the sum of the Pauling metallic radii ($r_{Sb}+r_{Ba}$=3.372 Å; $r_{Sb}+r_{Sb}$=2.782 Å) [29]. The less favourable distances to this interstitial Sb6 site are likely a result of matrix effects imposed

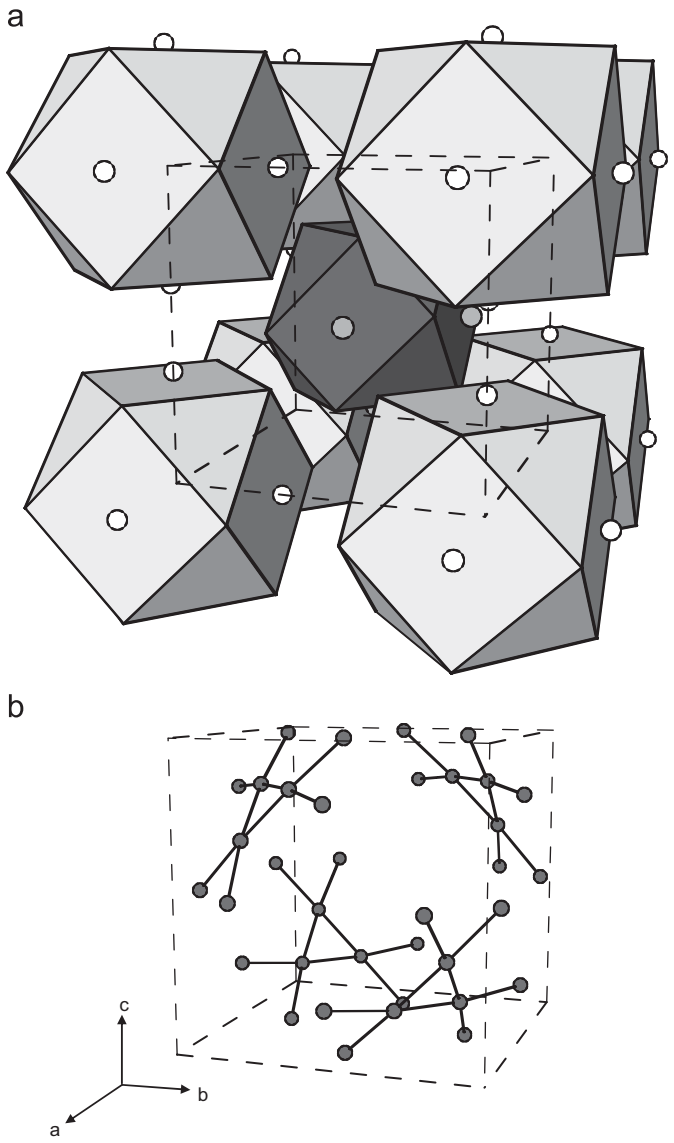

Fig. 2. The cubic unit cell of $Ba_5Ti_{12}Sb_{19+x}$ contains (a) two types of clusters (constructed from Ba and Sb atoms) in a CsCl-type arrangement and (b) planar Ti_9 clusters oriented parallel to {111}.

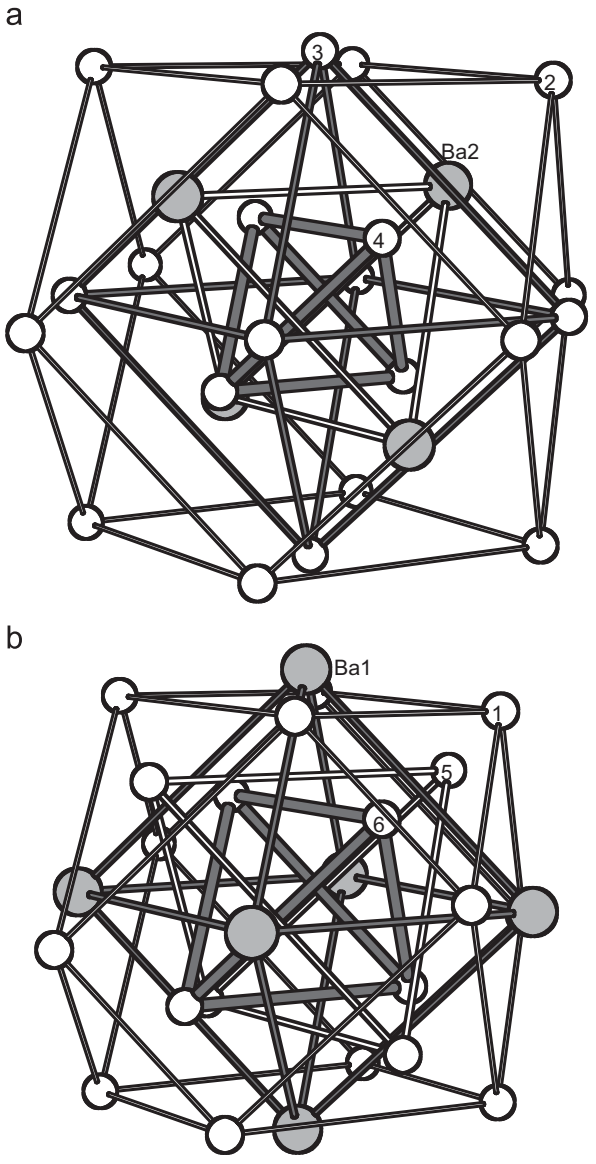

Fig. 3. The two types of 26-atom clusters, consisting of an inner tetrahedron (IT) within an outer tetrahedron (OT) within an octahedron (OH) within a cuboctahedron (CO). The Ba atoms are found in either (a) the OT or (b) the OH sites.

by the requirement to pack atoms densely within the γ-brass framework.

As a result of the face-sharing of $TiSb_6$ octahedra (in the conventional polyhedral description) in $Ba_5Ti_{12}Sb_{19+x}$, Ti atoms are brought into close proximity. Although the Ti–Ti distances (2.941–2.942 Å for the Ti1–Ti1 and Ti1–Ti2 contacts) are slightly longer than the sum of the metallic radii ($r_{Ti}+r_{Ti}$=2.648 Å) [29], they are comparable to those found in other Ti-containing antimonides in which metal–metal bonding is implicated (e.g., Ti_5Sb_3, 2.838–2.989 Å [30]; $La_2Ti_7Sb_{12}$, 2.920–3.059 Å [8]). In fact, many binary Ti–Sb and ternary *RE*–Ti–Sb phases are characterized by low-dimensional Ti substructures, in the form of butterfly clusters (Ti_5Sb_3 [30]), chains ($Ti_{11}Sb_8$ [31], $Sm_2Ti_{11-x}Sb_{14+x}$ [9]), and planar nets (Ti_2Sb [21], $La_2Ti_7Sb_{12}$ [8]). Only Ti_3Sb (tetragonal Cr_3Si-type structure) possesses a 3D framework built up from linked Ti_9 clusters (with Ti atoms centred within Ti_8 square antiprisms) [32]. The structure of $Ba_5Ti_{12}Sb_{19+x}$ can also be built up from Ti_9 clusters, but these are nearly planar and are oriented parallel to the four symmetry-equivalent members of the {111} form of crystal planes (Fig. 2b). Each cluster is constructed from three Ti1 atoms in a triangle, which is decorated by six attached Ti2 atoms (Fig. 4a). If the Ti2–Ti2 side (3.280 Å) is completed, then similar planar Ti_9 clusters can be identified as fragments of the kagome net found in the structure of $NdTi_3(Sb_{1-x}Sn_x)_4$ (Fig. 4b) [8]. Linking the Ti_9 clusters in $Ba_5Ti_{12}Sb_{19+x}$ results in a 3D 3- and 4-connected net with a unique topology, a projection of which can be seen in Fig. 1.

Although the composition of $Ba_5Ti_{12}Sb_{19+x}$ is quite high in Sb, there is little Sb–Sb bonding present in the structure. If the underoccupied Sb6 site is discounted, then the only possibly significant interaction is the rather long distance (3.281 Å) of the three Sb1 atoms surrounding an Sb5 atom in a trigonal plane (Fig. 4c).

An interesting conundrum is presented in trying to account for the electronic structure of $Ba_5Ti_{12}Sb_{19+x}$. The occurrence of the γ-brass substructure adopted by the Ba and Sb atoms suggests the application of Hume–Rothery electron concentration rules [10]. A valence electron concentration (vec) ranging from 20/13 to 22/13 is required to stabilize the γ-brass structure. Clearly the vec for $Ba_5Ti_{12}Sb_{19+x}$, in terms of any conceivable idealized formula for the full structure or the Ba–Sb substructure, far exceeds the permitted range. Two related compounds unexpectedly adopting the γ-brass structure are $Hf_{10}Ta_3S_3$ [33] and $Li_{21}Si_5$ [34]. In $Hf_{10}Ta_3S_3$, which is the only other known example of a stuffed γ-brass structure, the Hume–Rothery rules are preserved by invoking a reduced electron count (restricted to only s and p electrons) for Hf and Ta atoms and the donation of additional electrons by the S atoms [33]. In $Li_{21}Si_5$, the electronic structure is consistent not only with the Hume–Rothery rules but also with the Zintl–Klemm concept, if an extended formalism is invoked involving the use of Li cage orbitals [34]. Although the Hume–Rothery rules fail for $Ba_5Ti_{12}Sb_{19+x}$, application of the Zintl–Klemm concept does reveal that it is "nearly" a Zintl phase. If we initially assume the absence of any homoatomic Ti–Ti or Sb–Sb interactions, then the idealized formulation $(Ba^{2+})_5(Ti^{4+})_{12}(Sb^{3-})_{19}$ is almost electron-precise, with the charge of 58+ of the Ba and Ti atoms not quite compensated by the charge of 57- of the Sb atoms. To maintain charge neutrality, one solution would be to propose that the Ti atoms do not fully transfer their valence electrons, i.e., $(Ba^{2+})_5(Ti^{3.9+})_{12}(Sb^{3-})_{19}$. The availability of *d*-electrons on the Ti atoms then leads to the prediction of some residual Ti–Ti bonding, as observed. Another solution is the addition of excess Sb atoms, i.e., $(Ba^{2+})_5(Ti^{4+})_{12}(Sb^{3-})_{19.3}$. Reassuringly, the observed upper limit of the Sb non-stoichiometry corresponds to $Ba_5Ti_{12}Sb_{19.2}$.

The calculated band structure for idealized $Ba_5Ti_{12}Sb_{19}$ (neglecting the Sb6 site) reinforces these general conclusions. In

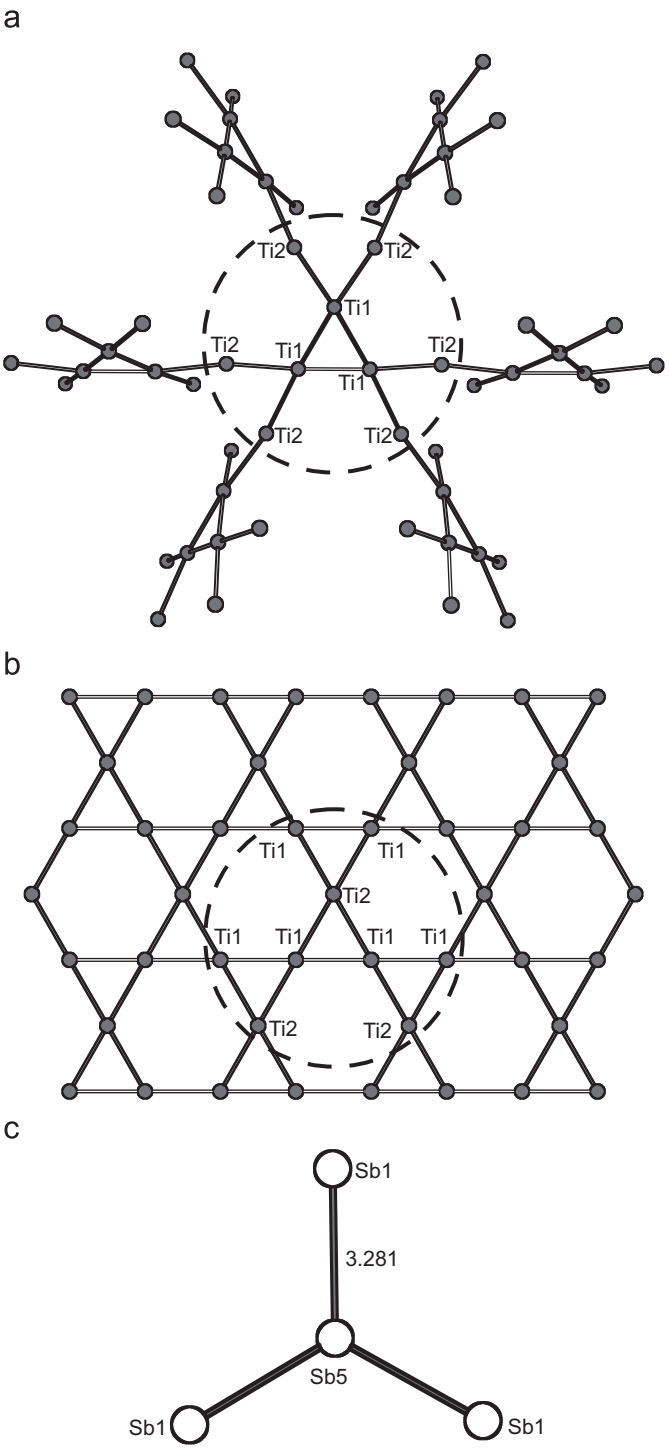

Fig. 4. Homoatomic bonding units. (a) Planar Ti_9 clusters are found in $Ba_5Ti_{12}Sb_{19+x}$, with each cluster connected to six others, and in (b) $NdTi_3(Sb_{1-x}Sn_x)_4$, as part of a kagome net. (c) A trigonal planar unit of Sb atoms is also found in $Ba_5Ti_{12}Sb_{19+x}$.

the density of states (DOS) curve, most of the Ba contributions lie above the Fermi level at 0 eV (Fig. 5a), supporting the notion of significant electron transfer from the Ba atoms and lending credence to the picture of a "polar" intermetallic compound. Most of the states below the Fermi level consist of contributions from the Ti and Sb atoms. The crystal orbital Hamilton population (COHP) curves for different contacts are shown in Fig. 5b. As expected, the heteroatomic Ti–Sb bonding interactions within the $TiSb_6$ octahedra are dominant (–ICOHP of 2.0 eV/bond), Ti–Ti

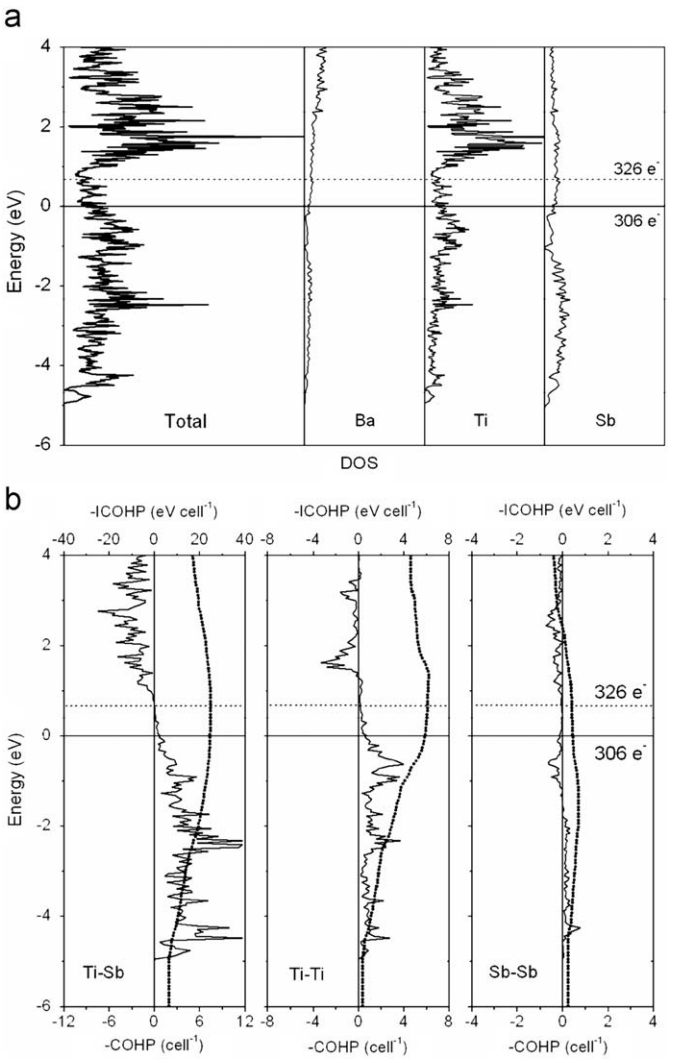

Fig. 5. (a) Density of states (DOS) and its Ba, Ti, and Sb projections for an idealized model "$Ba_5Ti_{12}Sb_{19+x}$" in which the Sb6 site is neglected. (b) Crystal orbital Hamilton population (COHP) curves (solid lines) and integrated COHP curves (dotted lines) for Ti–Sb, Ti–Ti, and Sb–Sb contacts. The Fermi levels corresponding to the electron counts for the idealized models $Ba_5Ti_{12}Sb_{19+x}$ (306 e^-/cell) and $Ba_5Ti_{12}Sb_{21}$ (326 e^-/cell) are marked.

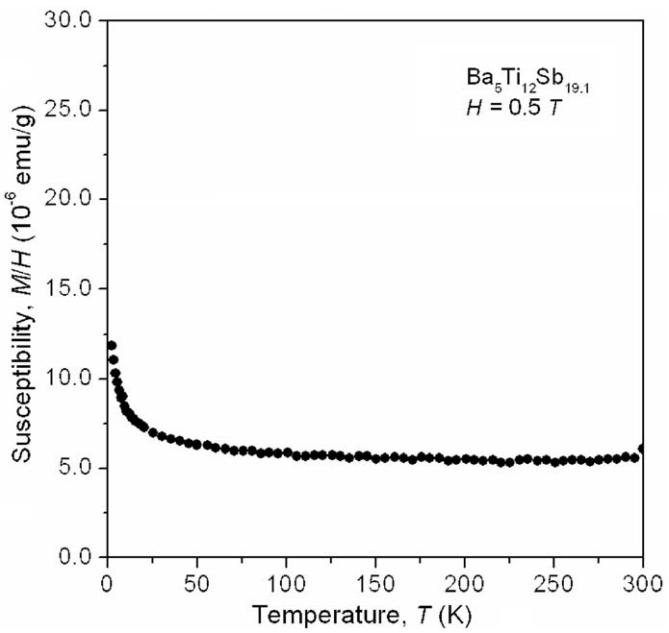

Fig. 6. Magnetic susceptibility for $Ba_5Ti_{12}Sb_{19.1}$.

bonding within the 3D Ti network is intermediate (1.5 eV/bond), and Sb–Sb bonding within the trigonal plane is very weak (0.4 eV/bond). Closer inspection of the Ti–Sb and Ti–Ti COHP curves reveals additional bonding states just above the Fermi level. Within the rigid band model, the prediction is that addition of a small number of electrons to the system will shift the Fermi level up slightly to fill these bonding states. A similar situation is observed in $AE_9Zn_{4+x}Sb_9$, in which additional Zn atoms can be inserted because of electronic reasons [35]. In fact, Ti–Sb and Ti–Ti bonding is optimized at 0.7 eV, at an electron count corresponding precisely to the formula "$Ba_5Ti_{12}Sb_{21}$" in which the Sb6 site is fully occupied. Counteracting this effect, however, Sb–Sb bonding is already optimized at −1.5 eV, at a much lower electron count, and these interactions become increasingly destabilized as antibonding states continue to be filled above the Fermi level. If the band structure calculation is performed on a hypothetical "$Ba_5Ti_{12}Sb_{21}$" model, the introduction of a fully occupied Sb6 site (generating short 2.8 Å Sb6–Sb1 distances) does contribute additional bonding stability (–ICOHP of 1.0 eV/bond) but, by virtue of new bonding interactions with the surrounding atoms, actually diminishes Ti–Sb (–ICOHP of 1.7 eV/bond) and Ti–Ti bonding (–ICOHP of 1.3 eV/bond). Although the reasons differ from the rigid band prediction above, the conclusion is the same: full occupation of the Sb6 site is disfavoured. These analyses, of course, neglect the contributions of Madelung energy and size effects (such as the highly distorted coordination environment offered by the Sb6 site), which will also influence the homogeneity range observed in $Ba_5Ti_{12}Sb_{19+x}$.

The dc magnetic susceptibility of $Ba_5Ti_{12}Sb_{19.1}$ exhibits an unremarkable temperature-independent paramagnetism, consistent with the absence of localized unpaired electrons in this metallic system (Fig. 6).

4. Conclusions

$Ba_5Ti_{12}Sb_{19+x}$ is an intermetallic compound that combines the structural characteristics of a Hume–Rothery phase (γ-brass Cu_9Al_4) with the electronic characteristics of a Zintl phase. The non-stoichiometry arises from weak occupation of an interstitial Sb site. It is the second example of a stuffed γ-brass structure in which a complex 3D Ti network of unique topology interweaves through an arrangement of 26-atom Ba–Sb clusters. We have made an attempt to rationalize the composition and bonding through simple electron-counting as well as band structure calculations, but recognize that other factors may be at work to influence the formation of this unusual structure.

Acknowledgments

The Natural Sciences and Engineering Research Council of Canada and the University of Alberta supported this work. We thank Dr. Robert McDonald and Dr. Michael J. Ferguson (X-ray Crystallography Laboratory) for the X-ray data collection, Ms. Christina Barker (Department of Chemical and Materials Engineering) for assistance with the EDX analysis, and Mr. Peter E.R. Blanchard for the XPS analysis.

Appendix A. Supplementary materials

Supplementary data associated with this article can be found in the online version at 10.1016/j.jssc.2009.08.030.

References

[1] S.M. Kauzlarich, S.R. Brown, G.J. Snyder, Dalton Trans. (2007) 2099–2107.
[2] V. Svitlyk, F. Fei, Y. Mozharivskyj, J. Solid State Chem. 181 (2008) 1080–1086.
[3] J. Xu, H. Kleinke, J. Comput. Chem. 29 (2008) 2134–2143.
[4] W.-Z. Cai, L.-M. Wu, L.-H. Li, L. Chen, Eur. J. Inorg. Chem. (2009) 230–237.
[5] G.A. Papoian, R. Hoffmann, Angew. Chem. Int. Ed. 39 (2009) 2408–2448.
[6] G. Bolloré, M.J. Ferguson, R.W. Hushagen, A. Mar, Chem. Mater. 7 (1995) 2229–2231.
[7] S.H.D. Moore, L. Deakin, M.J. Ferguson, A. Mar, Chem. Mater. 14 (2002) 4867–4873.
[8] H. Bie, S.H.D. Moore, D.G. Piercey, A.V. Tkachuk, O. Ya. Zelinska, A. Mar, J. Solid State Chem. 180 (2007) 2216–2224.
[9] H. Bie, A. Mar, Inorg. Chem. 47 (2008) 6763–6770.
[10] W. Hume-Rothery, G.V. Raynor, The Structure of Metals and Alloys, Institute of Metals, London, 1962.
[11] S.M. Kauzlarich (Ed.), Chemistry, Structure, and Bonding of Zintl Phases and Ions, VCH Publishers, New York, 1996.
[12] G.M. Sheldrick, SHELXTL, version 6.12, Bruker AXS Inc., Madison, WI, 2001.
[13] P. Villars (Ed.), Pauling File Binaries Edition, version 1.0, ASM International, Materials Park, OH, 2002.
[14] L.M. Gelato, E. Parthé, J. Appl. Crystallogr. 20 (1987) 139–143.
[15] R. Tank, O. Jepsen, A. Burkhardt, O.K. Andersen, TB-LMTO-ASA Program, version 4.7, Max Planck Institut für Festkörperforschung, Stuttgart, Germany, 1998.
[16] B. Saparov, S.-Q. Xia, S. Bobev, Inorg. Chem. 47 (2008) 11237–11244.
[17] A.P. Holm, M.M. Olmstead, S.M. Kauzlarich, Inorg. Chem. 42 (2003) 1973–1981.
[18] H. Kim, C.L. Condron, A.P. Holm, S.M. Kauzlarich, J. Am. Chem. Soc. 122 (2000) 10720–10721.
[19] D.M. Young, C.C. Torardi, M.M. Olmstead, S.M. Kauzlarich, Chem. Mater. 7 (1995) 93–101.
[20] D.T. Chow, R. McDonald, A. Mar, Inorg. Chem. 36 (1997) 3750–3753.
[21] S. Derakhshan, A. Assoud, K.M. Kleinke, E. Dashjav, X. Qiu, S.J.L. Billinge, H. Kleinke, J. Am. Chem. Soc. 126 (2004) 8295–8302.
[22] S. Westman, Acta Chem. Scand. 19 (1965) 1411–1419.
[23] O. von Heidenstam, A. Johansson, S. Westman, Acta Chem. Scand. 22 (1968) 653–661.
[24] L. Arnberg, S. Westman, Acta Crystallogr. Sect. A 34 (1978) 399–404.
[25] J.K. Brandon, R.Y. Brizard, W.B. Pearson, D.J.N. Tozer, Acta Crystallogr. Sect. B 33 (1977) 527–537.
[26] S. Thimmaiah, K.W. Richter, S. Lee, B. Harbrecht, Solid State Sci. 5 (2003) 1309–1317.
[27] W. Hornfeck, S. Thimmaiah, S. Lee, B. Harbrecht, Chem. Eur. J. 10 (2004) 4616–4626.
[28] O. Gourdon, D. Gout, D.J. Williams, T. Proffen, S. Hobbs, G.J. Miller, Inorg. Chem. 46 (2007) 251–260.
[29] L. Pauling, The Nature of the Chemical Bond, 3rd ed., Cornell University Press, Ithaca, NY, 1960.
[30] R. Berger, Acta Chem. Scand. A 31 (1977) 889–890.
[31] S. Bobev, H. Kleinke, Chem. Mater. 15 (2003) 3523–3529.
[32] A. Kjekshus, F. Grønvold, J. Thorbjørnsen, Acta Chem. Scand. 16 (1962) 1493–1510.
[33] G.A. Marking, H.F. Franzen, J. Am. Chem. Soc. 115 (1993) 6126–6130.
[34] R. Nesper, H.G. Von Schnering, J. Solid State Chem. 70 (1987) 48–57.
[35] S.-Q. Xia, S. Bobev, J. Am. Chem. Soc. 129 (2007) 10011–10018.